Brazilian Journal
of Chemical
Engineering

ISSN 0104-6632
Printed in Brazil
www.abeq.org.br/bjche

Vol. 30, No. 01, pp. 167 - 186, January - March, 2013

A SURFACE-RENEWAL MODEL OF CROSS-FLOW MICROFILTRATION

A. Hasan[1], C. R. Peluso[2], T. S. Hull[3], J. Fieschko[4] and S. G. Chatterjee[5*]

[1]Doubletree Papermill, 31201 W. Thayer Road, Gila Bend, Arizona 85337, USA.
[2]Bristol-Myers Squibb, 6000 Thompson Road, East Syracuse, New York 13057-5050, USA.
[3]Department of Chemical and Biological Engineering, 320 Furnas Hall,
State University of New York at Buffalo, Buffalo, New York 14260, USA.
[4]4266 Fraser Fir Drive, Manlius, New York 13104, USA.
[5]Department of Paper and Bioprocess Engineering, Phone: + 1-315-470-6517, Fax: + 1-315-470-6945,
SUNY College of Environmental Science and Forestry, 1 Forestry Drive, Syracuse, New York 13210, USA.
E-mail: schatterjee@esf.edu

(Submitted: November 28, 2011 ; Revised: May 23, 2012 ; Accepted: May 26, 2012)

Abstract - A mathematical model using classical cake-filtration theory and the surface-renewal concept is formulated for describing cross-flow microfiltration under dynamic and steady-state conditions. The model can predict the permeate flux and cake buildup in the filter. The three basic parameters of the model are the membrane resistance, specific cake resistance and rate of surface renewal. The model is able to correlate experimental permeate flow rate data in the microfiltration of fermentation broths in laboratory- and pilot-scale units with an average root-mean-square (RMS) error of 4.6%. The experimental data are also compared against the critical-flux model of cross-flow microfiltration, which has average RMS errors of 6.3, 5.5 and 6.1% for the cases of cake filtration, intermediate blocking and complete blocking mechanisms, respectively.
Keywords: Membrane filtration; Surface-renewal model; Critical-flux model; Microfiltration.

INTRODUCTION

Cross-flow membrane filtration is widely utilized in the chemical, food and biopharmaceutical industries, and is also becoming common in wastewater treatment and biofuel applications. In cross-flow filtration, the feed solution or suspension to be filtered flows under pressure along the surface of a porous membrane through which the liquid permeates in a direction perpendicular to the direction of the main flow. As time progresses, gel-polarization and cake layers build up on the membrane surface, which lead to a gradual decline of permeate flux with time.

Microfiltration is a common method of separation with wide applications as demonstrated by numerous industrial and biotech usages such as enzyme recovery (Kroner *et al.*, 1984; Le *et al.*, 1984; Marston *et al.*, 1984), hormone production (Shoner *et al.*, 1985), protein recovery (Titchener-Hooker *et al.*, 1991), and cell lysate recovery (Bailey and Meagher, 1997a, 1997b). During membrane operation, permeate flux decline is a common and persistent challenge and is believed to occur due to pore blocking, concentration polarization and cake-layer buildup (Wiesner *et al.*, 1992; Bai and Leow, 2002a, 2002b).

Over the years numerous models, some examples of which are offered below, have been proposed in the literature to describe the decline of permeate flux with time in microfiltration. It is well recognized that in cross-flow filtration there is a final nonzero permeate flux; in this it departs significantly from dead-end filtration. Stamatakis and Tien (1993) presented a concise and critical summary of the early work on cross-flow microfiltration. Combining cake

*To whom correspondence should be addressed

filtration theory with the concept of particle adhesion probability, they developed a model of cross-flow filtration which successfully correlated permeate-flux data in the filtration of suspensions of kaolin reported by Murkes and Carlsson (1988). Field *et al*. (1995) introduced the concept of critical flux for cross-flow microfiltration. They incorporated the effect of cross-flow into the constant-pressure, blocking filtration equation developed by Hermia (1982) for dead-end filtration and derived a general equation to represent the decline of permeate flux with time. Their model will be discussed in detail later in this paper. Koltuniewicz *et al.* (1995) presented data on cross-flow and dead-end microfiltration of oily-water emulsions; these were subsequently used by Arnot *et al.* (2000) to compare three different models of flux decline. They found that the model developed by Field *et al*. (1995) provided the best fit to the data and the dominant fouling mechanism was either incomplete pore blocking or cake formation. According to Song (1998), the first phase of flux decline in microfiltration is caused by pore blocking—a rapid process with barely one layer of particles sufficing to complete maximum blocking of the membrane. Once particles are retained within the membrane, the effective pore diameter becomes gradually smaller allowing a gel or cake layer to build, which generates a second layer of resistance to filtration. In this phase, cake resistance increases as the cake gets thicker and flux decline continues until the cake layer attains an equilibrium thickness when a steady-state (nonzero) plateau in the permeate flux is established. Song (1998) modeled the filtration as a dynamic process that occurs in three phases: a rapid initial drop, a slow decline and a steady-state phase, and presented a closed-form solution. Bai and Leow (2002a) studied a membrane filtration system within an activated-sludge wastewater bioreactor. Their experiments revealed that operational conditions in the bioreactor (aeration rate, mechanical mixing and circulation flow through the membrane unit) affected the size distribution of particles in the wastewater, which in turn influenced the performance of the filtration unit. Also, smaller particles were more detrimental in causing fouling. They proposed a simple model based on Darcy's law and introduced parameters such as cake resistance, a parameter dependent on the cake thickness and specific cake resistance, and affected by the liquid velocity. An expression for the transient cake thickness was derived from a mass balance of particles under the assumption that the cake thickness becomes constant at steady state. The three parameters in the model were the initial permeate flux, final (steady-state) permeate flux and specific cake resistance. Wiesner *et al*. (1992) proposed simple models to describe the variation of permeate flux with time when the limiting resistance was due to the membrane, pore blocking or cake layer; these models were subsequently applied by Lim and Bai (2003) to describe microfiltration of activated-sludge wastewater. Hwang *et al.* (2003) developed a model of cross-flow microfiltration of binary suspensions of fine particles and macromolecules; their model, which included the effect of fluid shear on the cake layer, compared favorably with their experimental data on permeate flux. Jegatheesan *et al.* (2009) found internal fouling (pore blocking) and external fouling (cake formation) to be responsible for flux decline in ultra- and microfiltration of sugarcane juice. Empirical models were used to describe complete blocking, partial blocking and cake filtration phenomena. Hwang *et al.* (2010) investigated the effect of particle softness on the filtration resistance and permeate flux. Softer particles are thought to allow greater cake compression and a tighter, lighter cake leading to drastic flux decay at short filtration times.

The present work presents a model of cross-flow microfiltration that uses the surface-renewal concept, which has the potential for a more realistic description of the transfer of suspended solids due to random, hydrodynamic impulses generated at the membrane surface (e.g., due to membrane roughness or by the use of spacers or turbulence promoters) compared to existing models (e.g., film and boundary-layer models), which do not account for the random and unstable structure of the region close to the membrane wall. Koltuniewicz and Noworyta (1994) list three types of forces that influence mass transport in the near-wall region: (a) inertial forces caused by membrane roughness, (b) drag forces that can stimulate chaotic movements of fluid elements in both laminar and turbulent flow, and (c) lifting forces caused by the 'lateral migration' of colloidal particles and fluid elements that lead to the phenomenon of 'flux paradox' (i.e., high permeate flux), which cannot be explained by the film model. The surface-renewal concept has been used to describe cross-flow ultrafiltration and microfiltration in a few publications (Koltuniewicz, 1992; Koltuniewicz and Noworyta, 1994; Koltuniewicz and Noworyta, 1995; Constenla and Lozano, 1996; Arnot *et al*., 2000; Chatterjee, 2010; Sarkar *et al.*, 2011). For example, the surface-renewal model of Koltuniewicz (1992) assumes that the unsteady-state permeate flux J(t) in a specific liquid element with an exposure time of t at the membrane surface (i.e., in a surface element) is

the same as that occurring in ultrafiltration in an unstirred batch cell, which is represented by the empirical equation

$$J(t) = (J_0 - J^*)e^{-At} + J^* \quad (1)$$

where J_0 is assumed to be either the initial value of the flux during batch ultrafiltration (Koltuniewicz, 1992) or the pure solvent (i.e., water permeability) flux (Koltuniewicz and Noworyta, 1994), J^* is the permeate flux after infinite time in batch ultrafiltration, and A is a parameter expressing the rate of flux decline. To determine the permeate flux in cross-flow ultrafiltration under unsteady-state conditions, Koltuniewicz and Noworyta (1994; 1995) postulated that liquid elements at the membrane surface had ages that could be characterized by the unsteady-state form of the age-distribution function of Danckwerts [see Eq. (10)], which when used with Eq. (1), gives

$$J_a(t_p) = (J_0 - J^*)\frac{S}{S+A}\frac{1-e^{-(S+A)t_p}}{1-e^{-St_p}} + J^* \quad (2)$$

where $J_a(t_p)$ is the age-averaged permeate flux when the process time is t_p. The parameter S (assumed to be constant) is the rate of renewal of liquid elements at the membrane surface, which is an increasing function of the velocity of the main flow as demonstrated empirically by Koltuniewicz (1992), Koltuniewicz and Noworyta (1994) and Koltuniewicz and Noworyta (1995); this feature will be discussed later in this work. It can also be thought of as a 'scouring' term which represents the removal of deposited material (Arnot *et al.*, 2000), and which depends upon the level of flow instability. Since in membrane units the bulk flow Reynolds number is usually in the transient regime, such flow instabilities would be laminar instabilities (quasi-periodic flows) rather than chaotic turbulence.

Letting $t_p \rightarrow \infty$ in Eq. (2) yields the limiting or steady-state flux J_{lim} in cross-flow filtration as

$$J_{lim} = J_a(t_p \rightarrow \infty) = (J_0 - J^*)\frac{S}{S+A} + J^* \quad (3)$$

Koltuniewicz (1992) and Koltuniewicz and Noworyta (1995) applied Eq. (3) to the ultrafiltration of skim milk and bovine serum albumin (BSA) solutions, and to the microfiltration of an oil-in-water emulsion in hollow-fiber and flat-plate membrane modules, whereas Constenla and Lozano (1996) used it to correlate the behavior of J_{lim} with transmembrane pressure drop in the ultrafiltration of apple juice in a hollow-fiber module. Equation (2) has been used by Koltuniewicz and Noworyta (1994) to correlate permeate-flux data in the ultrafiltration of skim milk in a hollow-fiber module under dynamic conditions and also by Arnot *et al*. (2000) to model microfiltration of oily-water emulsions.

The surface-renewal model of Koltuniewicz (1992) has the following features: (1) There are four parameters in the flux equation [Eq. (2)], i.e., J_0, J^*, A, and S, and (2) the flux equation is of a semi-empirical nature with A and J^* being determined from the flux decline observed in a batch or dead-end ultrafiltration experiment under similar conditions as those used during the cross-flow experiment. In an effort to remove these limitations, this paper presents a comprehensive model of cross-flow microfiltration using the surface-renewal concept and classical cake-filtration theory, which does not exist as yet in the literature to our knowledge. The model can predict the permeate flux and cake buildup on the membrane surface under dynamic and steady-state conditions. The model is also calibrated with experimental permeate-flux data on the microfiltration of fermentation broths in laboratory- and pilot-scale units, i.e., values of the model parameters, viz., R_m (membrane resistance), k_c (a parameter that is related to the specific cake resistance α) and S (rate of renewal of liquid elements at the membrane surface) are deduced.

SURFACE-RENEWAL MODEL OF CROSS-FLOW MICROFILTRATION

A schematic of cross-flow microfiltration is shown in Fig. 1. In the surface-renewal model developed in this work (Fig. 2), it is postulated that the dominant fouling mechanism responsible for permeate flux decline is cake formation. The phenomenon of pore blocking is assumed to occur during the first moments of filtration and its effects are included in the membrane resistance R_m, which is treated as an empirical parameter—a detailed discussion of this issue is presented later. Flow instabilities are assumed to continuously bring fresh liquid elements from the bulk liquid to the membrane-liquid interface on the feed side. A liquid element remains at the membrane surface for a definite time t after which it returns and re-mixes with the bulk liquid. Below or above the surface elements, the liquid is assumed to be well mixed where the concentration of solids is held constant at its bulk value c_b due to a high rate of transport (due

to flow instability) from this point to the bulk liquid. As time progresses, a cake layer builds up on the membrane surface, which causes a gradual decline in permeate flux until it reaches a steady value. In order to model this process, which is the chief objective of this paper, it is assumed that, during the residence time t of a liquid element at the membrane surface, permeate flux and cake accumulation in the surface element can be described by classical cake-filtration theory (McCabe *et al.*, 1993).

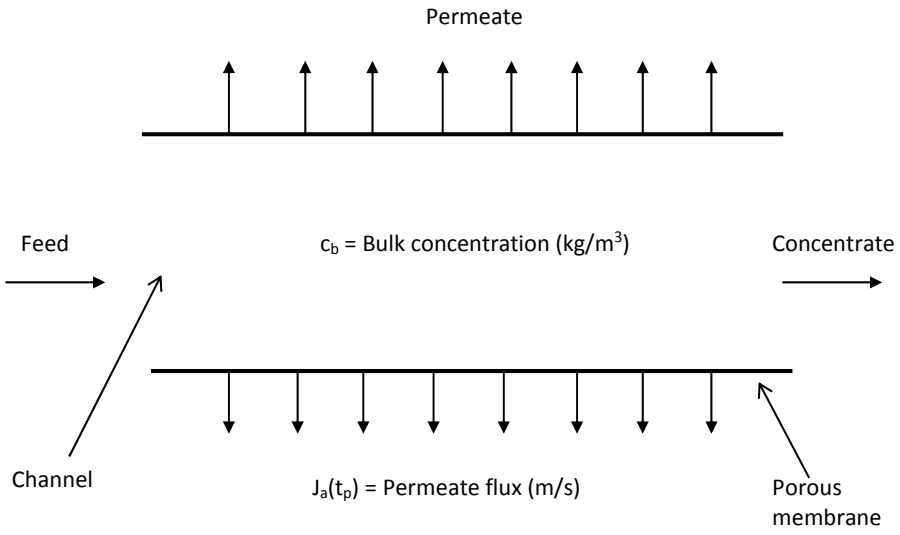

Figure 1: Schematic of cross-flow microfiltration.

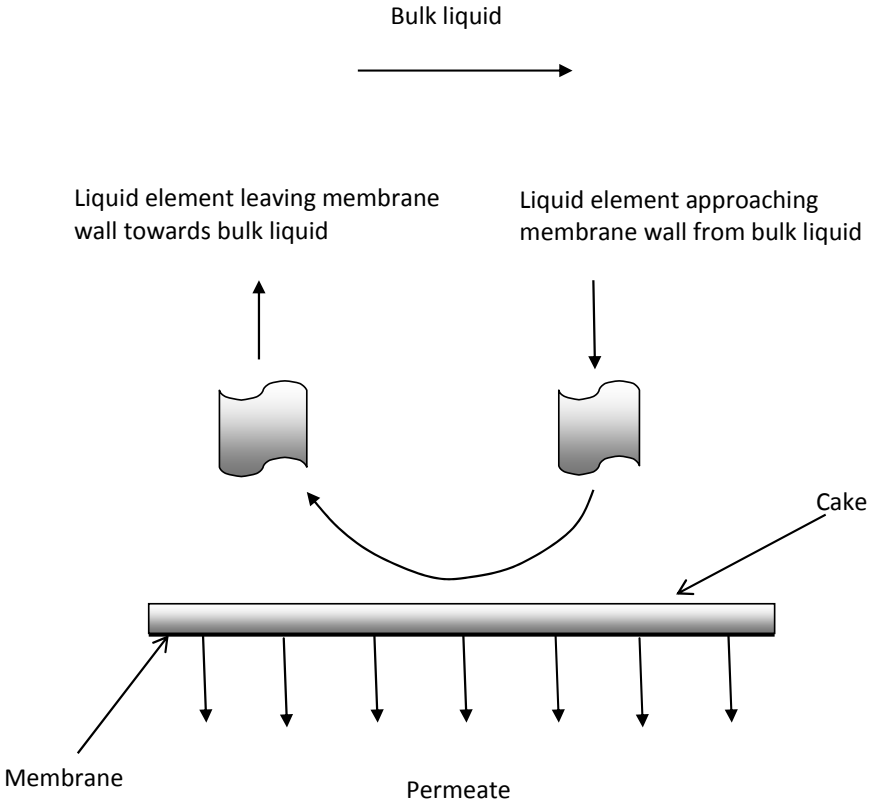

Figure 2: Surface-renewal mechanism.

This theory predicts a linear relationship between t/V and V where t is the time at which the total amount of filtrate collected is V. By algebraic manipulation of this relationship, it can be shown that the filtrate flux J(t) [= $(1/A_f)$ dV/dt with A_f being the filtration area] at time t (which, as mentioned above, is assumed to be equal to the permeate flux in a surface element with a residence time of t at the membrane wall in cross-flow microfiltration) is given by:

$$J(t) = \frac{1}{\sqrt{\left(1/J_0^2\right) + 2k_c t}} \tag{4}$$

where:

$$J_0 = \frac{\Delta p}{\mu R_m} \tag{5}$$

$$k_c = \frac{\mu c_b \alpha}{\Delta p} \tag{6}$$

In the above, J_0 is the permeate flux at time t = 0, Δp is the transmembrane pressure drop, μ is the viscosity of the filtrate, R_m is the resistance of the membrane or filter medium, c_b is the mass of solids deposited in the filter per unit volume of filtrate (same as the bulk or feed concentration of the suspension if the amount of liquid trapped in the pores of the wet cake is neglected) which is assumed to be constant, and α is the specific cake resistance.

The mass $m_c(t)$ of solids accumulated in the element during the time period of t per unit area of the membrane surface is expressed by:

$$m_c(t) = \int_0^t J(t) c_b dt \tag{7}$$

which, upon insertion of Eq. (4), becomes:

$$m_c(t) = \frac{c_b}{k_c}\sqrt{\left(1/J_0^2\right) + 2k_c t} - \frac{c_b}{k_c J_0} \tag{8}$$

At any time t_p during the filtration process, the surface of the membrane is visualized as being populated by a mosaic of liquid elements having different ages which range from zero to t_p. Denoting the age-distribution function of surface elements by $f(t, t_p)$, the age-averaged permeate flux (i.e., process flux) $J_a(t_p)$ at time t_p is given by:

$$J_a(t_p) = \int_0^{tp} J(t) f(t, t_p) dt \tag{9}$$

Assuming random surface renewal, Koltuniewicz and Noworyta (1994) derived a mathematical form for $f(t, t_p)$, a brief recapitulation of which is given in the appendix for the benefit of the reader. It may be shown that [see Eq. (A4)]:

$$f(t, t_p) = \frac{Se^{-St}}{1 - e^{-Stp}} \tag{10}$$

where S, as mentioned earlier, is the rate of renewal of liquid elements at the membrane surface. Substituting Eq. (10) into Eq. (9) gives:

$$J_a(t_p) = \int_0^{t_p} J(t) \frac{Se^{-St}}{1 - e^{-St_p}} dt \tag{11}$$

A question now arises on how to describe the nature of the cake formed on the membrane surface in a theoretical treatment. Either of the following two extreme assumptions may be made: (1) Flow instabilities extend right up to the membrane wall and the cake is visualized as a dynamic suspension of particles. Thus, in any new surface element, cake buildup starts from a "clean" membrane condition and J_0 is the same for all elements and independent of t_p. (2) Flow instabilities do not extend into the cake layer but only up to the outside edge of the cake. In a surface element of age t, the initial flux is equal to the value of the process flux at a process time of $t_p - t$, which will, therefore, not be the same for all surface elements. An actual situation will lie somewhere between these two extreme cases. Utilizing Eqs. (4) and (11) with the above assumptions yields the following two alternative formulations for $J_a(t_p)$, i.e.,

$$J_a(t_p) = \int_0^{t_p} \frac{1}{\sqrt{\left(1/J_0^2\right) + 2k_c t}} \frac{Se^{-St}}{1 - e^{-St_p}} dt \tag{12}$$

or

$$J_a(t_p) = \int_0^{t_p} \frac{1}{\sqrt{\left[1/(J_a(t_p - t))^2\right] + 2k_c t}} \frac{Se^{-St}}{1 - e^{-St_p}} dt \tag{13}$$

Equation (12) can be readily integrated to obtain $J_a(t_p)$ as an explicit function of t_p [see Eq. (17)]. In contrast, Eq. (13), which has to be integrated subject to the condition $J_a(t_p = 0) = J_0$, shows that the value of the process flux $J_a(t_p)$ at time t_p contains the entire history of this flux starting from $t_p = 0$. Both Eqs. (12) and (13) are analogous to a hologram, each point of which 'enfolds' or 'carries' the total information of an illuminated structure (Bohm, 2005). Since a change between an object and its holographic image is much more drastic than a simple, geometric transformation (translation, rotation or dilation), Bohm (2005) referred to it by the term 'metamorphosis', which is a change 'in which everything alters in a thorough going manner while some subtle and highly implicit features remain invariant.' According to Eq. (12), the process flux is a weighted average of the elemental fluxes, i.e., the direction is from the microscopic (elemental) to the macroscopic (process) domain. In contrast, Eq. (13) describes a situation in which the process and elemental fluxes co-determine one another i.e., there is a two-way communication or dialectical interplay between the microscopic and macroscopic domains, which is deeper and more profound philosophically. As the level of flow instability rises, one would expect the situation represented by Eq. (12) to become increasingly more tenable. In this paper, Eq. (12) will be used for reasons of mathematical simplicity.

By integrating Eq. (12) and defining the dimensionless quantities:

$$S^* = \frac{S}{2k_c J_0^2} \tag{14}$$

$$t_p^* = St_p \tag{15}$$

$$J_a^*(t_p^*) = \frac{J_a(t_p)}{J_0} \tag{16}$$

it may be shown that:

$$J_a^*(t_p^*) = \frac{e^{S^*}}{1 - e^{-t_p^*}} \sqrt{\pi S^*} \left[\operatorname{erf}\left(\sqrt{S^* + t_p^*}\right) - \operatorname{erf}\left(\sqrt{S^*}\right) \right] \tag{17}$$

As $t_p^* \to 0$, it follows from Eq. (17) and l'Hôpital's rule that:

$$J_a^*(t_p^* \to 0) = 1 \tag{18}$$

while as $t_p^* \to \infty$, Eq. (17) becomes:

$$J_a^*(t_p^* \to \infty) = \frac{J_a(t_p \to \infty)}{J_0} = \frac{J_{lim}}{J_0} = J_{lim}^* = e^{S^*} \sqrt{\pi S^*} \left[1 - \operatorname{erf}\left(\sqrt{S^*}\right) \right] \tag{19}$$

where, as mentioned before, J_{lim} is the value of the limiting or steady-state permeate flux (i.e., as $t_p \to \infty$).

The model parameters can be estimated by the following procedure. The membrane resistance R_m can be determined from the value of the initial flux J_0 and Eq. (5) while the dimensionless surface-renewal rate S^* can be calculated from the experimental value of J_{lim} and Eq. (19). The surface-renewal rate S can then be determined by fitting Eq. (17) to experimental data of transient permeate flux so as to minimize the root-mean-square (RMS) deviation between predicted and experimental values of the flux. Finally, k_c and α can be calculated from Eqs. (14) and (6), respectively.

In some situations, the value of J_0 can be high, i.e., $J_0 \to \infty$; Eq. (17) then simplifies to:

$$J_a(t_p) = J_{lim} \frac{\operatorname{erf}\left(\sqrt{St_p}\right)}{1 - e^{-St_p}} \tag{20}$$

where:

$$J_{lim} = \sqrt{\frac{\pi S}{2k_c}} \tag{21}$$

Equation (20) has the same form as the transient permeate flux in cross-flow ultrafiltration (Chatterjee, 2010). The value of S can be obtained from the experimental value of J_{lim} and by fitting Eq. (20) to permeate-flux data, after which α can be determined from Eqs. (21) and (6). Equation (21) shows that an increase in S (e.g., caused by an increase in the level of flow instability) and a decrease in k_c (say, due to an increase in the transmembrane pressure drop or by a reduction in feed concentration) will lead to an increase in the value of J_{lim}, which agrees with physical intuition. As mentioned earlier and as shown by Eq. (17), the permeate flux declines with time due to a gradual buildup of a cake of solids on the membrane surface. At time t_p after start of the

filtration process, the age-averaged mass of cake $m_{c,a}(t_p)$ accumulated per unit area of the membrane surface is given by:

$$m_{c,a}(t_p) = \int_0^{t_p} m_c(t) \frac{Se^{-St}}{1-e^{-St_p}} dt \tag{22}$$

Substituting Eq. (8) into Eq. (22) and integrating yields:

$$m^*_{c,a}(t^*_p) = \frac{e^{S^*}}{\left(1-e^{-t^*_p}\right)\sqrt{S^*}} \left[\Gamma\left(3/2, S^*\right) - \Gamma\left(3/2, S^* + t^*_p\right)\right] - 1 \tag{23}$$

where

$$m^*_{c,a}(t^*_p) = \frac{m_{c,a}(t_p) J_0 k_c}{c_b} \tag{24}$$

and $\Gamma(x, y)$ is the extended Euler gamma function defined by:

$$\Gamma(x,y) = \int_y^{\infty} \lambda^{x-1} e^{-\lambda} d\lambda \tag{25}$$

As $t^*_p \to 0$, using l'Hôpital's rule and Eq. (23) gives:

$$m^*_{c,a}(t^*_p \to 0) = 0 \tag{26}$$

while as $(t^*_p \to \infty)$, Eq. (23) becomes:

$$m^*_{c,a}(t^*_p \to \infty) = m^*_{c,\lim} = \frac{e^{S^*}}{\sqrt{S^*}} \Gamma\left(3/2, S^*\right) - 1 \tag{27}$$

which is the steady-state value of the dimensionless cake mass.

Equations (17) and (23) express the following: In dimensionless coordinates, the permeate flux and cake mass are functions of process time with the surface-renewal rate being the sole governing parameter. It can be shown from Eqs. (19) and (27) that, as $S^* \to 0$, $J^*_{\lim} \to 0$ and $m^*_{c,\lim} \to \infty$ while as $S^* \to \infty$, $J^*_{\lim} \to 1$ and $m^*_{c,\lim} \to 0$. Equations (19) and (27), which are universal functions, are plotted in Fig. 3.

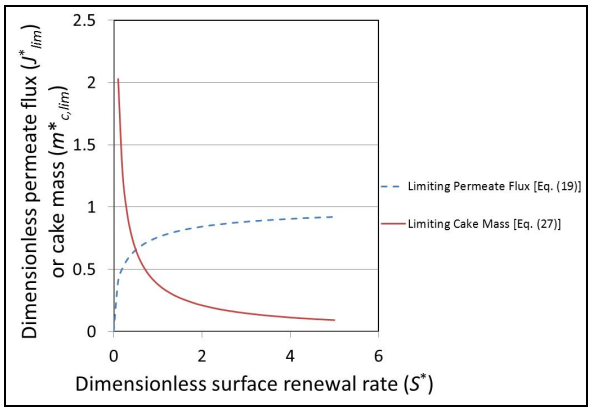

Figure 3: Behavior of steady-state permeate flux and cake buildup as a function of surface-renewal rate in dimensionless coordinates.

CRITICAL-FLUX MODEL OF CROSS-FLOW MICROFILTRATION

The general equation of the critical-flux model can be expressed as (Field *et al*., 1995):

$$-\frac{dJ}{dt_p} J^{n-2} = k(J - J_{crit}) \tag{28}$$

where k is a constant and n equals 0, 1, 1.5, and 2 for cake filtration, intermediate blocking, standard blocking, and complete blocking mechanisms, respectively. J_{crit} is the critical flux, which is the value of the permeate flux below which a decline of flux with time does not occur, and whose value depends upon the prevailing hydrodynamics and other factors. For cake filtration (i.e., n = 0), Eq. (28) reduces to:

$$-\frac{1}{J^2}\frac{dJ}{dt_p} = k(J - J_{crit}) \tag{29}$$

whose solution, subject to the condition that at $t_p = 0$, $J = J_0$, is (Field *et al*., 1995)

$$kt_p = \frac{1}{J^2_{crit}}\left[\ln\left(\frac{J}{J_0}\left(\frac{J_0 - J_{crit}}{J - J_{crit}}\right)\right) - J_{crit}\left(\frac{1}{J} - \frac{1}{J_0}\right)\right] \tag{30}$$

which is an implicit equation for the permeate flux as a function of process time, in contrast to the explicit form for the surface-renewal model, as may be seen from Eq. (17). From Eq. (30) it is apparent that there are three parameters in the critical-flux model: J_0, J_{crit} and k. J_0 can be expressed in terms of R_m and Δp

through Eq. (5). According to Eq. (28), $dJ/dt_p = 0$ at $J = J_{crit}$ and, since this is expected to occur as $t_p \rightarrow \infty$, it has been assumed in this work that J_{crit} is equal to the experimental value of the limiting or steady-state flux, J_{lim} (see also Arnot *et al*., 2000). The third parameter k can then be obtained from the slope of a plot of the right-hand-side of Eq. (30) as a function of t_p. It is to be noted that k and J_{crit} can be expressed in terms of more fundamental parameters (Field *et al*., 1995), i.e.,

$$k = \frac{\alpha K_{cake}}{J_0 R_m} \tag{31}$$

$$J_{crit} = \frac{E}{K_{cake}} \tag{32}$$

where K_{cake} is a cake-filtration constant (a function of certain physical properties) and E is the rate of cake erosion per unit area. Thus, according to Eq. (32) [which is analogous to Eq. (21) of the surface-renewal model], an increase in E (say, due to an increase in the liquid velocity or level of flow instability) and a decrease in K_{cake} will lead to an increase in J_{crit} (i.e., the limiting or steady-state flux). Since Field *et al.* (1995) did not provide any definition for K_{cake}, it was not possible to calculate values of the basic quantities α, E, and K_{cake} from the values of J_{crit} and k, which were obtained from experimental permeate-flux data as described earlier.

For n = 1 (intermediate blocking), the solution of Eq. (28) is given by (Field *et al*., 1995):

$$kt_p = \frac{1}{J_{crit}} \ln\left[\frac{J}{J - J_{crit}}\left(\frac{J_0 - J_{crit}}{J_0}\right)\right] \tag{33}$$

The parameter k can be estimated from the slope of a plot of the right-hand-side of Eq. (33) versus t_p with R_m and J_{crit} being obtained as mentioned earlier.

For n = 2 (complete blocking), the solution of Eq. (28) is (Field *et al*., 1995):

$$-kt_p = \ln\left(\frac{J - J_{crit}}{J_0 - J_{crit}}\right) \tag{34}$$

where

$$k = \frac{\sigma J_0}{\varepsilon_0} \tag{35}$$

with σ and ε_0 being the blocked area per unit volume of filtrate and initial membrane surface porosity, respectively. The slope of a plot of the right-hand-side of Eq. (34) versus t_p will yield k.

The standard blocking (n = 1.5) model is not considered in this work since it does not include back transport from the membrane wall (Field *et al*., 1995).

EXPERIMENTAL DETAILS

Cross- or tangential-flow filtration is often employed in the bioprocess industry to separate microbial cells from the liquid following cell growth in a fermenter. The permeate flow rate is known to depend on the transmembrane pressure drop and velocity of the liquid across the membrane surface.

Fermentation

Fermentation was carried out on two different scales. For filtration runs with the small- or laboratory-scale membrane unit (Fig. 4), a 15-L fermenter was used that contained aerobically grown (1) *Escherichia coli* (rod-shaped bacteria), (2) *Burkholderia cepacia* (of elliptical shape) and (3) *Pichia stipitis* (a hat-shaped yeast) that are used to produce ethanol, polyhydroxyalkanoates and ethanol, respectively. The glucose minimal salts medium in which the growth occurred was supplemented with complex nutrients. For runs with the pilot-scale cross-flow unit shown in Fig. 5, the broth was generated by (1) anaerobic fermentation of *Candida pseudotropicalis* using cheese whey as the nutrient medium and (2) aerobic growth of the same organism on a glycerol growth medium, both in a 400-L fermenter. During fermentation, an environment of controlled pH, temperature, agitation, and dissolved oxygen (in case of aerobic runs) was maintained.

Membrane Characteristics

Laboratory-scale and pilot-scale ceramic micro-filtration units manufactured by Hilliard Corporation, Elmira, New York, were used in this work. The small- scale unit consisted of three tubular ceramic membrane modules with pH resistance of 2–13 and thermal resistance of 0–149 °C. The cylindrical membrane modules (2.54 cm diameter) were 30.48 cm long and contained numerous channels (~ 60) of square cross-section having a side of approximately 0.18 cm. The modules came in pore sizes of 0.01, 0.2 and 0.45 μm, and had a total membrane surface area of 0.13 m^2. This unit (0.01 and 0.2 μm pore size) was also used by Hasan *et al*. (2011) for separating hydrolyzate components in the hot-water extract of sugar maple wood.

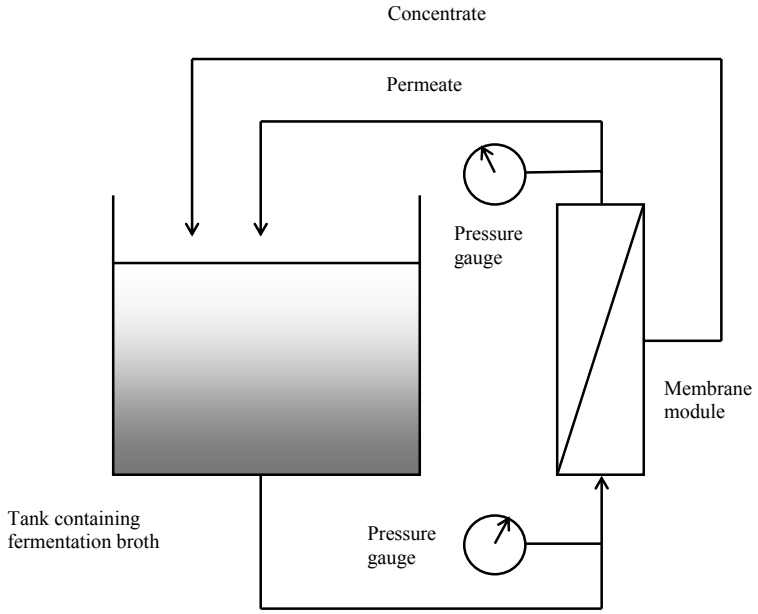

Figure 4: Schematic representation of the laboratory-scale microfiltration unit.

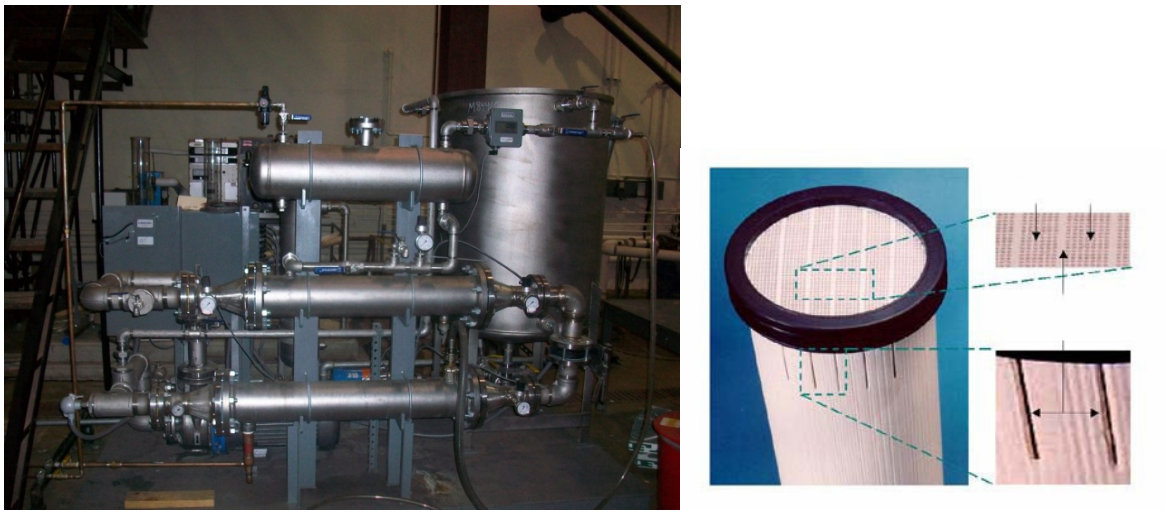

Figure 5: Pilot-scale microfiltration unit (Hilliard Corporation, Elmira, New York).

The pilot-scale membrane unit had 1800 channels with an average pore size of 0.2 μm; each channel was 86.36 cm long and had a square cross-section with a side of 0.18 cm. Some channels were converted to permeate conduits, which allowed the entire filter diameter to be effectively utilized. The total membrane filtration area was 11.15 m^2 with the membrane having the following operating characteristics: Maximum Δp = 413.7 kPa, maximum inlet pressure = 586.1 kPa, maximum differential pressure = 206.8 kPa, and maximum back pulse pressure = 689.5 kPa.

Experimental Runs

Tangential-flow filtration runs were performed in total recycle mode, i.e., permeate and retentate were both continuously recirculated back to the feed vessel. In the small unit, the filtration was performed over a 2-h period. At the end of the run, the filter was sometimes back pulsed and then removed from its housing for soaking in 0.25 N alkali solution. Thereafter, it was put back into its housing and run through with alkali solution and rinsed several times with water. During filtration, the

temperature was controlled by running cold water through a jacket (not shown in Fig. 4) around the vessel so as to prevent a change in liquid viscosity due to an increase in temperature. In the pilot-scale unit, a filtration run lasted for 1 h on average. The cleaning of the filter module was accomplished by back pulsing and rinsing with water and alkali solution.

RESULTS AND DISCUSSION

The ability of the surface-renewal model was tested by fitting it to the data of permeate flow rate in the cross-flow microfiltration of the fermentation broths mentioned above. The value of the viscosity μ of the filtrate necessary to calculate R_m from Eq. (5) was assumed to be the same as that of water at the experimental temperature (McCabe *et al*., 1993; Perry *et al*., 1984), i.e., the effects of substrate and salts on the viscosity were neglected. The characteristics of the fermentation broths, experimental conditions and details of the membrane modules used in the experiments are reported in Table 1.

Figure 6 shows the behavior of the clean-water flux at 20 °C as a function of Δp for the small-scale unit for two different membrane pore sizes. The data can be fitted reasonably well with straight lines, and from the slopes of the plots, Eq. (5) and using a value of 0.0011 kg/(m.s) for the viscosity of water at 20 °C (Perry *et al*., 1984), the values of R_m for the clean membrane are estimated to be 1.14×10^{12} and 1.01×10^{12} m^{-1} for membrane pore sizes of 0.2 and 0.45 μm, respectively. The data for the 0.2 μm membrane pore size has been previously reported by Hasan *et al*. (2011).

Table 1: Characteristics of the fermentation broths, experimental conditions and details of the membrane modules used in the cross-flow microfiltration runs.

Expt. no. and cell type	Fermentation medium and type	Initial optical density of broth @ 540 nm	Temp. °C	Δp kPa	Membrane unit type and area (m^2)	Membrane pore size (μm)	Membrane type
1. *Escherichia coli*	glucose aerobic	53	21.8	206.84	small 0.13	0.45	ceramic
2. *Burkholderia cepacia*	glucose aerobic	82	21.5	206.84	small 0.13	0.45	ceramic
3. *Pichia stipitis*	glucose aerobic	72	22.8	206.84	small 0.13	0.45	ceramic
4. *Candida pseudotropicalis*	cheese whey anaerobic	3	35.7	291.30	pilot 11.15	0.2	ceramic
5. *Candida pseudotropicalis*	glycerol aerobic	66	46.9	207.60	pilot 11.15	0.2	ceramic

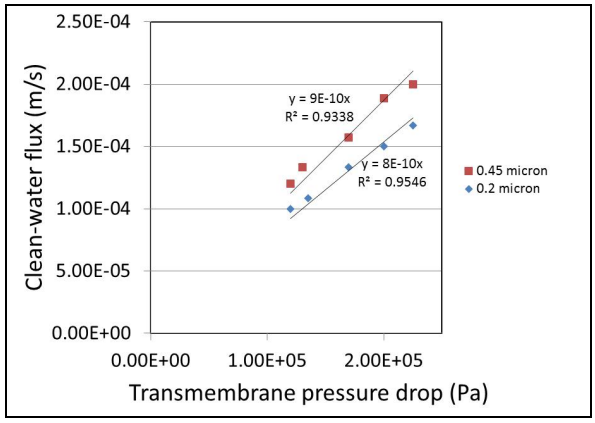

Figure 6: Clean-water flux at 20 °C in the small-scale unit.

Figures 7 and 8 compare the predictions of the surface-renewal model with data of permeate flow rate from the small- and pilot-scale units, respectively. The method used to determine the optimum values of the three parameters (R_m, k_c and S) has been explained earlier—these, along with RMS deviations between theoretical and experimental permeate flow rates, are shown in Table 2. The higher the values of R_m and k_c, the lower is the permeate flux [Eq. (4)]. Of the three types of cells used in the filtration runs in the small-scale unit, *P. stipitis* has the lowest value of k_c followed by *B. cepacia* and *E. coli*, respectively, the value for *P. stipitis* being about 11 times lower than that for *E. coli*. This implies a great difference in the nature of the cake formed from these different types of cells. For the large-scale unit, the values of k_c are of comparable magnitude since they are for the same type of cell (*C. pseudotropicalis*), albeit grown under two different conditions. The value of the surface-renewal rate *S* varies from 3.0–5.1 × 10^{-4} s^{-1} (average: 4.4 × 10^{-4} s^{-1}) in the small-scale unit and 7.5–10.1 × 10^{-4} s^{-1} (average: 8.8 × 10^{-4} s^{-1}) in the large-scale unit, which can be compared with the range of 8.4–17.4 × 10^{-4} s^{-1} found by Chatterjee (2010) for the experimental permeate-flux data of Koltuniewicz and Noworyta (1994) in the ultrafiltration of skim milk in a hollow-fiber membrane module (Romicon HF-15-43-PM 50) at 30 °C. Koltuniewicz and Noworyta (1994) had reported a range of 14–25.4 × 10^{-4} s^{-1} for the same data in their version of the surface-renewal model.

The following observations can be drawn from Figs. 7–8 and Tables 1–2: (1) There is good agreement between theoretical and experimental permeate flow rates with the average RMS deviation between predicted and experimental values being 4.6%. (2) The experimental flux declines with process time and attains a steady-state or limiting value as predicted by the model [Eq. (17)]. (3) The experimental values of the initial permeate flux J_0, which is usually believed to be the pure solvent flux of the membrane (Koltuniewicz and Noworyta, 1994), are not the same for the different experimental runs—this is reflected by the varying values of R_m in Table 2, which are approximately 4 to 19 times greater than the value of R_m of the clean membrane for the small-scale unit.

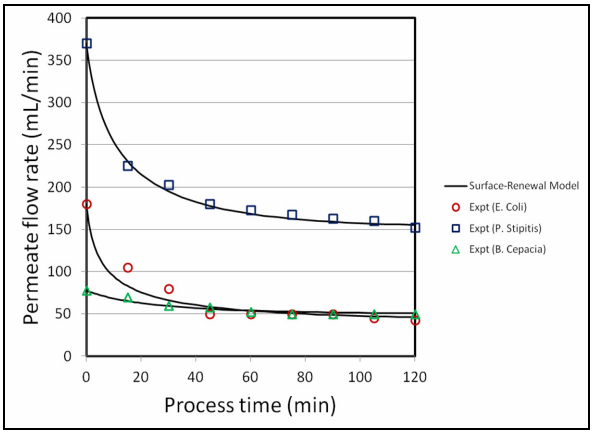

Figure 7: Comparison of the surface-renewal [calculated from Eq. (17)] and experimental permeate flow rates in the microfiltration of fermentation broths in the small-scale unit. Values of the model parameters are provided in Table 2.

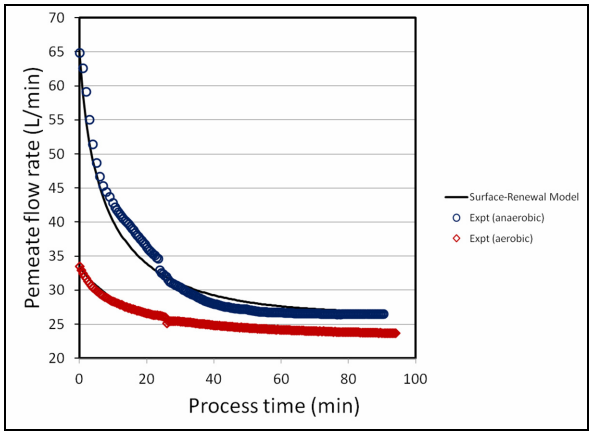

Figure 8: Comparison of the surface-renewal [calculated from Eq. (17)] and experimental permeate flow rates in the microfiltration of *Pseudo tropicalis* in the pilot-scale unit. Values of the model parameters are provided in Table 2.

Table 2: Parameter values of the surface-renewal model for the cross-flow microfiltration runs of Table 1.

Expt. no. and cell type	$R_m \times 10^{-13}$ m^{-1}	$k_c \times 10^{-6}$ $s\ m^{-2}$	$S \times 10^4$ s^{-1}	RMS error %
1. *Escherichia coli*	0.812	11.323	3.0	12.0
2. *Burkholderia cepacia*	1.922	5.531	5.1	3.6
3. *Pichia stipitis*	0.368	1.063	5.0	2.5
4. *Candida pseudotropicalis*	0.109	0.391	7.5	4.0
5. *Candida pseudotropicalis*	0.0895	0.285	10.1	0.9
Average				4.6

Also, for the small-scale unit, R_m varies by a factor of 5.2 whereas, for the pilot-scale unit, the factor is 1.2. The following hypotheses can be advanced for this behavior: (a) the procedure used to clean the membrane module between experimental runs was not adequate, or pore blocking had occurred in the initial moments of filtration. For the two runs in the pilot-scale unit that involved *C. pseudotropicalis*, it is observed that the value of R_m is about 22% higher for the run under anaerobic conditions in which Δp was 40% greater compared to the run under aerobic conditions (Tables 1 and 2). This may be in part due to the additional forcing of solids in the broth into the membrane because of the higher permeate flux (Fig. 8) caused by the greater Δp (McCabe *et al*., 1993). The values of R_m in Table 2 are thus derived from a fouled membrane and not a clean one. In conventional cake filtration theory, no complete analysis of the buildup of the (initial) resistance of the filter cloth is possible since this resistance will depend on how the pressure is developed and on the support geometry; it is hence usual to combine the resistance of the cloth with that of the first few layers of deposited particles, which have a propensity to block the pores of the cloth (Richardson *et al*., 2002). (b) The viscosity of water (at the experimental temperature) was used in this work to calculate R_m. However, the actual viscosity of the filtrate may have been different due to biological activity, which is a function of the cell type and fermentation conditions, and by the presence of substrate and salts in the growth medium. (c) Fouling of the membrane during the initial moments of filtration was dependent on the type of cells in the broth. This explains the large variation in R_m for the small-scale unit in which three different types of cells were used as compared to the pilot-scale unit in which only cell type was used. (d) Table 1 shows that the initial optical density of the different broths varied to a considerable extent.

In the microfiltration of sugar-maple wood extract, Hasan *et al*. (2011) found a significant difference between values of the initial permeate flux J_0 and the clean-water flux, which they attributed to a difference in viscosity. Huang and Morrissey (1998) observed that J_0, which they called the apparent initial permeate flux, depended on feed concentration—the higher this concentration, the lower was the initial flux. According to them, it is difficult to measure the true initial permeate flux because it is not possible to stabilize the system pressure instantaneously as the feed is pumped into the filter. The first measurement point can be obtained only after some 'lag' time that depends upon the measurement technique according to Koltuniewicz (1992), who recommended that pure solvent permeability measurements, after correction for the osmotic pressure effect, be used to calculate J_0 in the case of ultrafiltration. This points to uncertainty associated with experimental data of permeate flux near the beginning of filtration. In light of these considerations, it is best to treat R_m as an empirical parameter, which would also include any resistance to flow in the pipes to and from the filter (McCabe *et al*., 1993). Arnot *et al*. (2000), in their modeling of microfiltration, also used J_0 as an adjustable parameter in order to minimize experimental errors in the initial flow rate measurement—although they found that in most cases it was not significantly different from the clean-water flux under equivalent operating conditions.

Since only the optical density (OD) at 540 nm of the feed suspension was measured (Table 1) and not the actual cell concentration c_b, it was not possible to calculate values of the cake mass $m_{c,a}$. However, if it is assumed, as a very approximate measure, that 1 OD unit corresponds to 0.5 kg/m^3, then the steady-state values of the cake mass are calculated to be 0.58, 1.26 and 2.12 kg/m^2 for *E. coli*, *B. cepacia* and *P. stipitis*, respectively, for the small-scale unit, which are rough estimates and may not be precise. Figures 9 and 10 illustrate the growth of the dimensionless cake mass $m^*_{c,a}$ as a function of the dimensionless process time t^*_p in the small- and pilot-scale units, respectively, for the different broths as calculated from Eq. (23). All the curves start at a value of zero and develop towards steady state as t^*_p increases. The values of the dimensionless steady-state permeate flux J^*_{lim}, dimensionless steady-state cake mass $m^*_{c,lim}$ and dimensionless surface-renewal rate S^* are provided in Table 3 for all the experimental runs reported in this work. It can be seen that as S^* increases, J^*_{lim} increases towards a value of 1 due to a decrease in $m^*_{c,lim}$ (see also Fig. 3).

The surface-renewal model presented in this paper is self-contained, i.e., the three model parameters can be completely determined (in a sequential manner) by fitting the model to experimental permeate-flux data. Two of the parameters (membrane and cake resistances) are from conventional cake filtration theory while the third (surface-renewal rate) depends upon the hydrodynamic state in the channel.

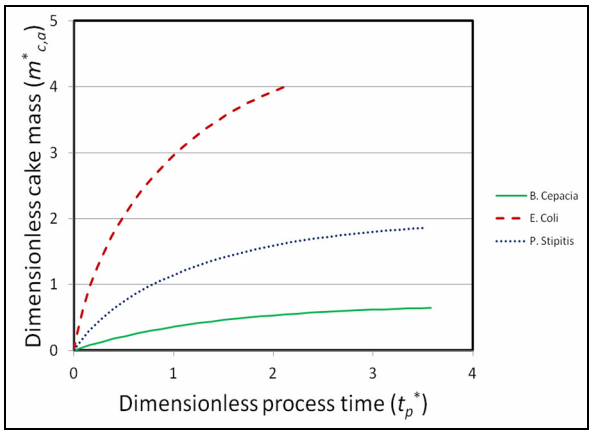

Figure 9: Predicted cake buildup with process time by the surface-renewal model [Eq. (23)] in the microfiltration of fermentation broths in the small-scale unit. Values of the dimensionless surface-renewal rate S^* are given in Table 3.

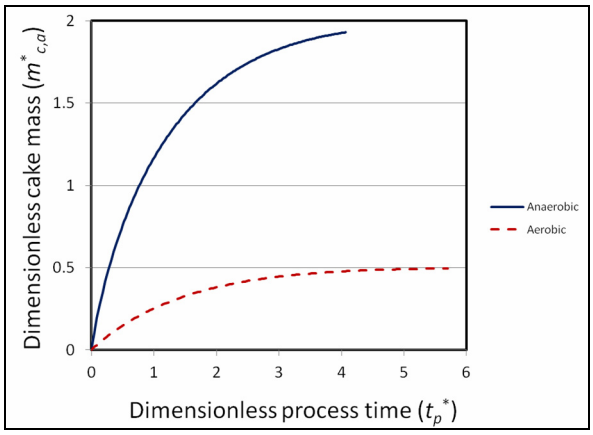

Figure 10: Predicted cake buildup with process time by the surface-renewal model [Eq. (23)] in the microfiltration of *Pseudo tropicalis* in the pilot-scale unit. Values of the dimensionless surface-renewal rate S^* are given in Table 3.

Table 3: Dimensionless quantities of the surface-renewal model for the cross-flow microfiltration runs of Table 1.

Expt. No. and cell type	$J^*_{lim} \times 10$	$m^*_{c,lim}$	$S^* \times 10$
1. *Escherichia coli*	2.36	4.74	0.25
2. *Burkholderia cepacia*	6.45	0.69	4.67
3. *Pichia stipitis*	4.12	1.97	1.05
4. *Candida pseudotropicalis*	4.09	2.00	1.02
5. *Candida pseudotropicalis*	7.08	0.50	7.07

As mentioned earlier, S can be correlated with the liquid velocity u in the main flow direction through the membrane channel, which was precluded in this work since the feed flow rate was not measured. Koltuniewicz and Noworyta (1995) used the surface-renewal model to determine the variation of S with u for milk ultrafiltration, BSA concentration and microfiltration of dodecane-water emulsions in hollow-fiber and flat-plate modules. Table 4 reports their experimental details and correlations of S as a function of u. It can be seen that S is a power-law function of u, with the exponent of u being greater than 1 in the case of microfiltration and less than 1 for ultrafiltration. Koltuniewicz and Noworyta (1995) attributed this to the dominance of the lateral migration effect in case of the former and the existence of transient flow regimes in case of the latter in the modules which they used.

Table 4: Experimental details and correlations for the surface renewal-rate S from the work of Koltuniewicz and Noworyta (1995).

Experimental details	ROMICON	UFMOD	PLEIADE
Module type	Hollow fiber	Flat plate	Flat plate
Membrane type	Polysulfone	PVC	CERAMESH 0.1
Membrane area (m^2)	1.4	1×10^{-2}	0.54×10^{-2}
Cross-flow area (m^2)	5×10^{-4}	10^{-4}	0.62×10^{-4}
Hydraulic diameter (m)	1.2×10^{-3}	2×10^{-3}	1×10^{-3}
Solute	Skimmed milk	BSA	Dodecane emulsion
Concentration	0–85 g/L	0–50 g/L	0–1000 ppm
Transmembrane pressure drop, Δp (kPa)	0–180	0–180	0–120
Cross-flow velocity, u (m/s)	0–0.65	0–2	0–1.2
Temperature (°C)	25	25	25
Surface-renewal rate, S (s^{-1})	$S = 3.48 \times 10^{-3}\ u^{0.661}$	$S = 0.748 \times 10^{-3}\ u^{0.75}$	$S = 0.459 \times 10^{-3}\ u^{4.464}$

In a prior study of ultrafiltration of a BSA solution in a flat-plate module, Koltuniewicz (1992) presented data that showed an almost linear relationship of S with u over a range of u = 0.1−1.6 m/s (corresponding to a Reynolds number range of 100−1600) and also found that S was independent of Δp. From standard mass-transfer coefficient correlations for flow in a tube (Rautenbach and Albrecht, 1989; Koltuniewicz and Noworyta, 1994), it can be deduced that S varies with u raised to a power that ranges from 0.66−1.75 as the flow changes from laminar to turbulent. Equation (21) predicts that the limiting or steady-state flux in cross-flow microfiltration is proportional to $S^{0.5}$, which result also holds for cross-flow ultrafiltration (Chatterjee, 2010). Thus, the limiting flux should be proportional to $u^{0.33}$ for laminar flow and $u^{0.875}$ in the case of turbulent flow. This conclusion agrees closely with the observation made by Rudolph and MacDonald (1994) that for modules that operate in the laminar flow regime, the flux increases as the one-third power of the tangential flow rate (or shear), while for devices operating in the turbulent flow regime, the flux increases in proportion to the tangential flow rate. If it is assumed that the main flow velocity in the small-scale unit was 1.3 m/s (from Table 1 of Hasan *et al*., 2011), the correlation in Table 4 for the flat-plate module UFMOD (whose hydraulic diameter D of 2 mm is comparable to the value of 1.8 mm for our system) predicts a value of S equal to 9.1×10^{-4} s^{-1}, which can be compared with the average value of 4.4×10^{-4} s^{-1} mentioned earlier for the small-scale unit. From dimensional considerations it may be postulated that:

$$\frac{SD}{u} = a\left(\frac{Du\rho_s}{\mu_s}\right)^b \tag{36}$$

where ρ_s and μ_s are the density and viscosity of the feed suspension, respectively, while a and b are parameters, with a being dependent on the module configuration (Koltuniewicz and Noworyta, 1995). The values of b are − 0.339, − 0.25 and 3.464 for the ROMICON, UFMOD and PLEIADE modules in Table 4. Equation (36) can be generalized to include the effect of membrane roughness δ as:

$$\frac{SD}{u} = g(Re, \delta/D) \tag{37}$$

where Re (= $Du\rho_s/\mu_s$) is the Reynolds number. In honor of Koltuniewicz, who pioneered the use of the surface-renewal concept in cross-flow membrane filtration, it is proposed that the dimensionless group SD/u be henceforth named as the Koltuniewicz number (Ko).

Figures 11 and 12 compare the predictions of the critical-flux model for the case of n = 0 [cake filtration; Eq. (30)] with permeate flow rate data from the small- and pilot-scale units, respectively. The optimum values of the three parameters (R_m, k and J_{crit}), along with RMS deviations between theoretical and experimental permeate flow rates, are reported in Table 5.

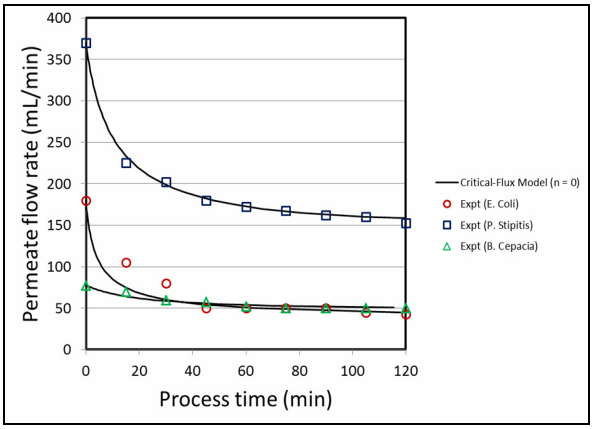

Figure 11: Comparison of the critical-flux [n = 0; calculated from Eq. (30)] and experimental permeate flow rates in the microfiltration of fermentation broths in the small-scale unit. Values of the model parameters are provided in Table 5.

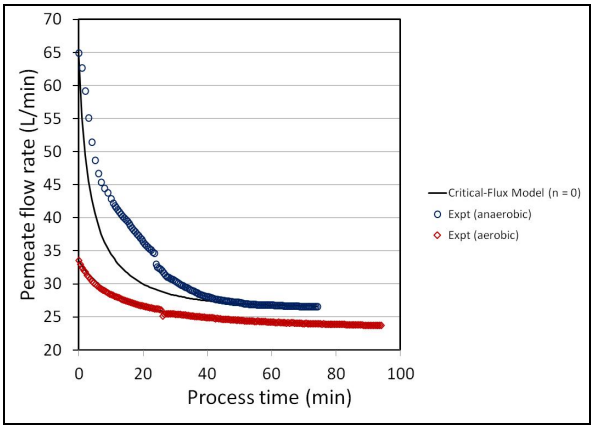

Figure 12: Comparison of the critical-flux [n = 0; calculated from Eq. (30)] and experimental permeate flow rates in the microfiltration of *Pseudo tropicalis* in the pilot-scale unit. Values of the model parameters are provided in Table 5.

Table 5: Parameter values of the critical-flux model (n = 0) for the cross-flow microfiltration runs of Table 1.

Expt. No. and cell type	$R_m \times 10^{-13}$ m^{-1}	$k \times 10^{-6}$ $s\ m^{-2}$	$J_{crit} \times 10^{6}$ $m\ s^{-1}$	RMS error %	r^2 value of fit of Eq. (30)
1. *Escherichia coli*	0.812	9.0	5.446	14.9	0.847
2. *Burkholderia cepacia*	1.922	9.0	6.407	4.6	0.876
3. *Pichia stipitis*	0.368	0.830	1.954	1.7	0.997
4. *Candida pseudotropicalis*	0.109	0.610	3.961	9.9	0.887
5. *Candida pseudotropicalis*	0.0895	0.538	3.549	0.6	0.995
Average				6.3	0.920

It is observed (as in the case of the surface-renewal model) that, in general, there is fair agreement between the theoretical and experimental values of the permeate flow rate, with the average RMS deviation between predicted and experimental values being 6.3%. For Runs 1, 2 and 4, the RMS errors are significantly greater compared to those for Runs 3 and 5—reflected in higher values of the correlation coefficient r^2 for these runs. Although not shown here, the experimental data, when plotted in the form of Eq. (30), yielded nearly perfect straight lines for Runs 3 and 5, while for Runs 2 and 4 they exhibited a distinct curvature.

Figures 13 and 14 show comparisons of the critical-flux model for the case of n = 1 [intermediate blocking; Eq. (33)] with permeate flow rate data from the small- and pilot-scale units, respectively, while Table 6 reports optimum values of the model parameters along with RMS deviations between the theoretical and experimental permeate flow rates. Overall, the intermediate blocking model [Eq. (33)], which has an average RMS deviation of 5.5%, is in closer agreement with the experimental data compared to the cake-filtration model [Eq. (30)].

Finally, Figs. 15–16 and Table 7 present results for the critical-flux model for the case of n = 2 [complete blocking; Eq. (34)]. Although the average RMS error of the fit is 6.1%, which is lower than the case for n = 0, Field *et al.* (1995) did not recommend the use of this model unless the fouling mechanism could be described by the equations used to derive Eq. (34), which is a difficult proposition to test by direct empirical observation.

If one were to adopt the critical-flux point of view, which postulates that there is a single, dominant fouling mechanism throughout each of the filtration experiments (Arnot *et al*., 2000), then one is forced to conclude from Tables 5–7 that the chief fouling mechanism was cake filtration in Runs 3 and 5, intermediate blocking in Run 1, and complete blocking in Runs 2 and 4. However, such a conclusion, which may have been appropriate in the case of an ideal feed suspension containing particles of uniform size and shape, would be simplistic in the case of this work, which used aqueous suspensions of bacterial, yeast or fungal cells as the feed.

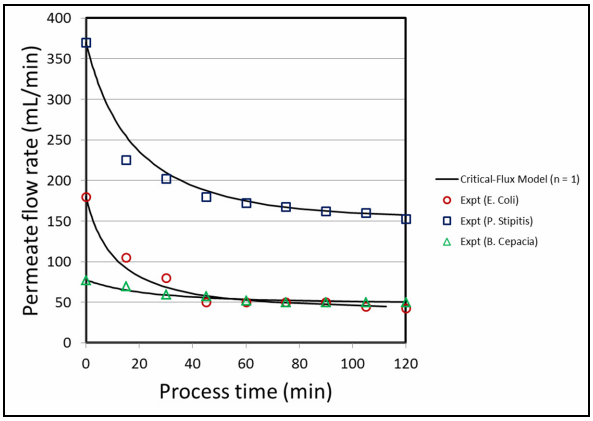

Figure 13: Comparison of the critical-flux [n = 1; calculated from Eq. (33)] and experimental permeate flow rates in the microfiltration of fermentation broths in the small-scale unit. Values of the model parameters are provided in Table 6.

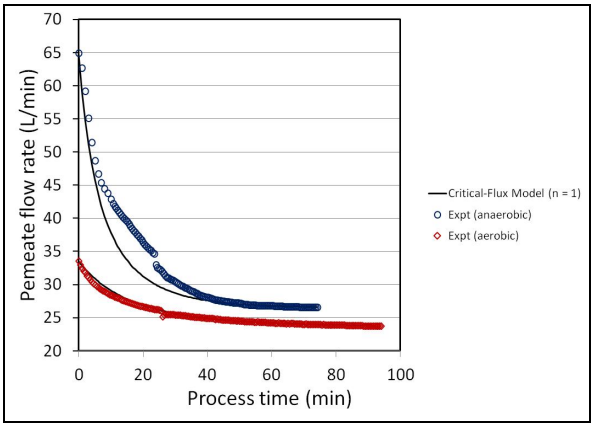

Figure 14: Comparison of the critical-flux [n = 1; calculated from Eq. (33)] and experimental permeate flow rates in the microfiltration of *Pseudo tropicalis* in the pilot-scale unit. Values of the model parameters are provided in Table 6.

Table 6: Parameter values of the critical-flux model (n = 1) for the cross-flow microfiltration runs of Table 1.

Expt. no. and cell type	$R_m \times 10^{-13}$ m^{-1}	k m^{-1}	$J_{crit} \times 10^6$ m s^{-1}	RMS error %	r^2 value of fit of Eq. (33)
1. *Escherichia coli*	0.812	71.224	5.446	9.9	0.874
2. *Burkholderia cepacia*	1.922	73.785	6.407	4.1	0.910
3. *Pichia stipitis*	0.368	21.738	1.954	5.4	0.975
4. *Candida pseudotropicalis*	0.109	28.644	3.961	7.0	0.937
5. *Candida pseudotropicalis*	0.0895	21.568	3.549	1.1	0.990
Average				5.5	0.937

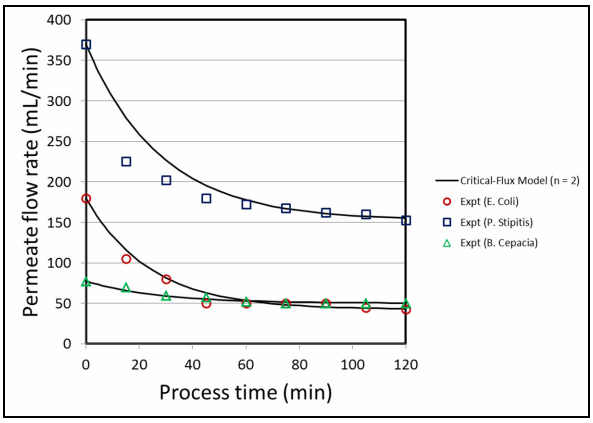

Figure 15: Comparison of the critical-flux [n = 2; calculated from Eq. (34)] and experimental permeate flow rates in the microfiltration of fermentation broths in the small-scale unit. Values of the model parameters are provided in Table 7.

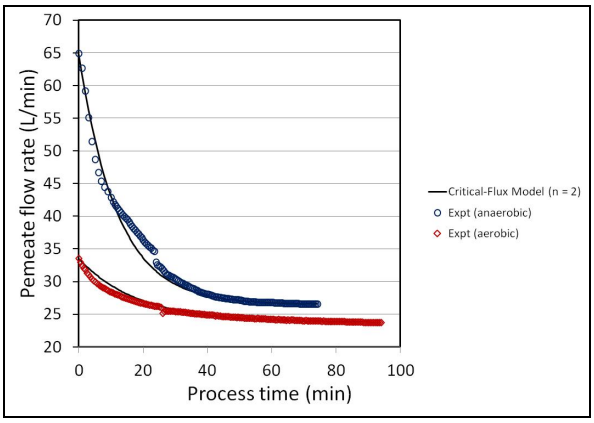

Figure 16: Comparison of the critical-flux [n = 2; calculated from Eq. (34)] and experimental permeate flow rates in the microfiltration of *Pseudo tropicalis* in the pilot-scale unit. Values of the model parameters are provided in Table 7.

Table 7: Parameter values of the critical-flux model (n = 2) for the cross-flow microfiltration runs of Table 1.

Expt. No. and cell type	$R_m \times 10^{-13}$ m^{-1}	$k \times 10^4$ s^{-1}	$J_{crit} \times 10^6$ m s^{-1}	RMS error %	r^2 value of fit of Eq. (34)
1. *Escherichia coli*	0.812	7	5.446	11.7	0.841
2. *Burkholderia cepacia*	1.922	6	6.407	3.5	0.941
3. *Pichia stipitis*	0.368	6	1.954	10.7	0.896
4. *Candida pseudotropicalis*	0.109	14	3.961	3.1	0.983
5. *Candida pseudotropicalis*	0.0895	9	3.549	1.6	0.974
Average				6.1	0.927

It is possible that the cells were not of uniform size and shape after fermentation and that cell fragments were generated due to cell lysis and the pumping action during filtration. The smaller fragments would block the pores of the membrane while the larger entities in the feed would cause cake formation, processes which could occur in parallel. Both the surface-renewal model, which (as stated earlier) postulates the dominant fouling mechanism to be cake formation with pore blocking occurring in the first moments of filtration, and the critical-flux model, which incorporates different fouling mechanisms (through the value of the parameter n), are highly idealized pictures of a very complex process. Comparing the surface-renewal and critical-flux (n = 0, 1) models reveals that the largest errors for both models occur for Runs 1 and 4.

CONCLUDING REMARKS

This work has presented a new model of cross-flow microfiltration that is based on the surface-renewal concept. The model, which assumes that the

chief fouling mechanism causing permeate flux decline is cake formation, is able to correlate experimental permeate flow rate data in the microfiltration of fermentation broths in laboratory- and pilot-scale units. Values of R_m, k_c and S, which are the three parameters of the model, range from 0.09–1.92 × 10^{13} m^{-1}, 0.29–11.32 × 10^6 s m^{-2} and 3.0–10.1 × 10^{-4} s^{-1}, respectively, in the filtration of fermentation broths used in the experiments reported herein. In contrast to the approach of Koltuniewicz (1992), Koltuniewicz and Noworyta (1994) and Koltuniewicz and Noworyta (1995), the surface-renewal model developed in this work is based on classical or conventional cake-filtration theory and has three parameters, all of which can be estimated from a single, cross-flow filtration experimental run.

The cake-filtration (n = 0), intermediate-blocking (n = 1) and complete blocking (n = 2) versions of the well-known critical flux model were also compared against the experimental data. Amongst these, the intermediate-blocking mechanism is in best overall agreement with the data and has an average RMS deviation of 5.5%, which is greater than the value of 4.6% of the surface renewal-model. It should be borne in mind, however, that the data reported in this work are the result of single experimental runs—it is difficult to reproduce fermentation broths of the same quality. Thus, the predictions of both models may lie within the range of the experimental error. Although it is not possible to arrive at a firm conclusion regarding the chief fouling mechanism, from a practical point of view, there is not much of a difference between the surface-renewal and critical-flux (n = 1) models in their ability to represent the experimental data presented here. These models, each one of which has three parameters, are based on different speculative hypotheses or constructions, which are not easy to verify directly. The surface-renewal and critical-flux models are essentially different interpolation techniques of representing the curve of permeate flux as a function of time, given the initial and long-time or steady-state values of the flux. Such models fall in the category of constructive theories, and as discussed recently by Chatterjee (2012), there can be more than one such theory that agrees with experimental data to within a prescribed degree of tolerance.

The surface-renewal model, which provides explicit expressions for the permeate flux and cake mass as functions of process time [see Eqs. (17) and (23)], in contrast to the critical-flux (n = 0, 1) model, is presented to the membrane community as an alternative theoretical description of cross-flow microfiltration. A more rigorous experimental protocol than that used in this work should be followed in order to test the model's ability to predict the influence of variables like transmembrane pressure drop, feed concentration and liquid velocity on the permeate flux. Further refinements to the model would consider the effects of cake compressibility and length of the filter module.

ACKNOWLEDGEMENTS

The authors gratefully acknowledge the help of Mr. Joseph Perrotta with the experimental work involving fermentation. S.G.C also thanks Mr. Susumu Ikuta and Dr. Noshir Mistry for throwing light on permeate-flux behavior in the tangential-flow microfiltration of fermentation broths.

NOMENCLATURE

a	parameter in Eq. (36)	
A	constant in Eq. (1) expressing rate of permeate-flux decline with time	s^{-1}
A_f	Filtration area in cake filtration	m^2
b	parameter in Eq. (36)	
c_b	mass of solids deposited in the filter per unit volume of filtrate (approximately equal to the concentration of solids in the feed or bulk liquid)	kg m^{-3}
D	hydraulic diameter of membrane channel	m
E	rate of cake erosion per unit area	kg m^{-2} s^{-1}
$f(t, t_p)$	age-distribution function of liquid elements at the membrane wall	s^{-1}
g	function of Re and δ/D [Eq. (37)]	
J(t)	instantaneous permeate flux in a surface element at time t or process flux in critical-flux model	m s^{-1}
J^*	permeate flux after infinite time in batch ultrafiltration	m s^{-1}
$J_a(t_p)$	age-averaged permeate flux when the process time is t_p	m s^{-1}
$J_a^*(t_p^*)$	dimensionless age-averaged permeate flux when the dimensionless process time is t_p^*	

J_{crit}	critical permeate flux	m s^{-1}
J_{lim}	limiting or steady-state permeate flux	m s^{-1}
J^*_{lim}	dimensionless limiting or steady-state permeate; J_{lim}/J_0	
J_0	initial permeate flux	m s^{-1}
k	parameter in critical-flux model	s m^{-2} (n = 0), m^{-1} (n = 1), s^{-1} (n = 2)
k_c	defined by Eq. (6)	s m^{-2}
K_{cake}	cake filtration constant in critical-flux model	kg m^{-3}
Ko	Koltuniewicz number (= SD/u)	
$m_c(t)$	mass of cake in a surface element per unit area of membrane surface at time t	kg m^{-2}
$m_{c,a}(t_p)$	age-averaged cake mass per unit area of membrane surface at process time t_p	kg m^{-2}
$m^*_{c,a}(t^*_p)$	dimensionless age-averaged cake mass when the dimensionless process time is t^*_p	
$m^*_{c,lim}$	limiting or steady-state dimensionless cake mass	
n	index in critical-flux model; equals 0, 1, 1.5 or 2 depending upon the fouling mechanism	
r^2	correlation coefficient	
R_m	hydraulic resistance of the membrane	m^{-1}
Re	Reynolds number (= $Du\rho_s/\mu_s$)	
S	rate of renewal of liquid elements at the membrane surface	s^{-1}
S^*	dimensionless surface-renewal rate defined by Eq. (14)	
t	time of exposure of a liquid element at the membrane surface	s
t_p	process time	s
t^*_p	dimensionless process time; defined by Eq. (15)	
V	total volume of filtrate collected during time t in cake filtration	m^3
u	liquid velocity in the main flow direction through the membrane channel	m s^{-1}
x	parameter of Γ(x, y)	
y	parameter of Γ(x, y)	

Greek Symbols

α	specific cake resistance	m kg^{-1}
Γ(x, y)	extended Euler gamma function; defined by Eq. (25)	
δ	membrane roughness	m
Δp	transmembrane pressure drop	Pa or kPa
ε_0	initial membrane surface porosity	
λ	variable of integration in Eq. (25)	
μ	viscosity of the permeate	kg m^{-1} s^{-1}
μ_s	viscosity of the feed suspension	kg m^{-1} s^{-1}
ρ_s	density of the feed suspension	kg m^{-3}
σ	blocked area per unit volume of filtrate	m^{-1}

REFERENCES

Arnot, T. C., Field, R. W. and Koltuniewicz, A. B., Cross-flow and dead-end microfiltration of oily-water emulsions. Part II: Mechanisms and modeling of flux decline. J. Membrane Sci., 169, 1-15 (2000).

Bai, R. and Leow, H. F., Microfiltration of activated sludge wastewater – the effect of system operation parameters. Sep. Purif. Technol., 29, 189-198 (2002).

Bai, R. and Leow, H. F., Modeling and experimental study of microfiltration using a composite module. J. Membrane Sci., 204, 359-377 (2002).

Bailey, S. M. and Meagher, M. M., The effect of denaturants on the crossflow membrane filtration of *Escherichia Coli* lysates containing inclusion bodies. J. Membrane Sci., 131, 29-38 (1997).

Bailey, S. M. and Meagher, M. M., Crossflow microfiltration of recombinant *Escherichia Coli* lysates after high pressure homogenization. Biotechnol. Bioeng., 56, 304-310 (1997).

Bohm, D., Wholeness and the Implicate Order. Routledge, London (2005).

Chatterjee, S. G., The nature of scientific theory. Current Science, 102, 386-388 (2012).

Chatterjee, S. G., On the use of the surface-renewal concept to describe cross-flow ultrafiltration. Indian Chemical Engineer, 52, 179-193 (2010).

Constenla, D. T. and Lozano, J. E., Predicting stationary permeate flux in the ultrafiltration of apple juice. Lebensm. Wiss. u. Technol., 29, 587-592 (1996).

Field, R. W., Wu, D., Howell, J. A. and Gupta, B. B., Critical flux concept for microfiltration fouling. J. Membrane Sci., 100, 259-272 (1995).

Hasan, A., Yasarla, R., Ramarao, B. V. and Amidon, T. E., Separation of lignocellulosic hydrolyzate components using ceramic microfilters. J. Wood Chem. Technol., 31, 357-383 (2011).

Hermia, J., Constant pressure blocking filtration laws. Application to Power-law non-Newtonian fluids. Trans. Ind. Chem. Eng., 60, 183-187 (1982). [*apud* Field *et al*. (1995).]

Huang, L. and Morrissey, M. T., Fouling of membranes during microfiltration of surimi wash water: Roles of pore blocking and surface cake formation. J. Membrane Sci., 144, 113-123 (1998).

Hwang, K.-J., Cheng, Y.-H. and Tung, K.-L., Modeling of cross-flow microfiltration of fine particle/macromolecule binary suspension. J. Chem. Eng. Japan, 36, 1488-1497 (2003).

Hwang, K-J., Wang, Y-T., Iritani, E. and Katagiri, N., Effect of gel particle softness on the performance of cross-flow microfiltration. J. Membrane Sci., 365, 130-137 (2010).

Jegatheesan, V., Phong, D. D., Shu, L. and Aim, R. B., Performance of ceramic micro- and ultrafiltration membranes in treating limed and partially clarified sugar cane juice. J. Membrane Sci., 327, 69-77 (2009).

Koltuniewicz, A., Predicting permeate flux in ultrafiltration on the basis of surface renewal concept. J. Membrane Sci., 68, 107-118 (1992).

Koltuniewicz, A. B., Field, R. W. and Arnot, T. C., Cross-flow and dead-end microfiltration of oily-water emulsion. Part I: Experimental study and analysis of flux decline. J. Membrane Sci., 102, 193-207 (1995).

Koltuniewicz, A. and Noworyta, A., Dynamic properties of ultrafiltration systems in light of the surface renewal theory. Ind. Eng. Chem. Res., 33, 1771-1779 (1994).

Koltuniewicz, A. and Noworyta, A., Method of yield evaluation for pressure-driven membrane processes. Chem. Eng. J., 58, 175-182 (1995).

Kroner, K. H., Schutte, H., Hustedt, H. and Kula, M., Cross-flow filtration in the downstream processing of enzymes. Process Biochem., 19, 67-74 (1984).

Le, M. S., Spark, L. B., Ward, P. S. and Ladwa, N., Microbial asparanginase recovery by membrane processes. J. Membrane Sci., 21, 307-319 (1984).

Lim, A. L. and Bai, R., Membrane fouling and cleaning in microfiltration of activated sludge wastewater. J. Membrane Sci., 216, 279-290 (2003).

Marston, F. A. O., Lowe, P. A., Doel, M. T., Schoemaker, S., White, S. and Angal, S., Purification of calf prochymosin (prorennin) synthesized in *Escherichia coli*. Nature Biotechnology, 2, 800-804 (1984).

McCabe, W. L., Smith, J. C. and Harriott, P., Unit Operations of Chemical Engineering. Fifth Ed., McGraw-Hill, New York (1993).

Murkes, J. and Carlsson, C. G., Cross Flow Filtration: Theory and Practice. John Wiley & Sons, New York (1988). [*apud* Stamatakis and Tien (1993).]

Perry, R. H., Green, D. W. and Maloney, J. O., Eds., Perry's Chemical Engineers' Handbook. Sixth Ed., McGraw-Hill, New York (1984).

Rautenbach, R. and Albrecht, R., Membrane Processes. John Wiley & Sons, New York (1989).

Richardson, J. F., Harker, J. H. and Backhurst, J. R., Coulson and Richardson's Chemical Engineering. Vol. 2, Fifth Ed., Butterworth-Heinemann, Oxford, UK (2002).

Rudolph, E. A. and MacDonald, J. H., Tangential Flow Filtration Systems for Clarification and Concentration, in Bioprocess Engineering: Systems, Equipment and Facilities. Lydersen, B. K., D'Elia, N. A. and Nelson, K. L., Eds., p. 119-157, John Wiley & Sons, Inc., New York (1994).

Sarkar, D., Datta, D., Sen, D. and Bhattacharjee, C., Simulation of continuous stirred rotating disk-membrane module: An approach based on surface renewal theory. Chem. Eng. Sci., 66, 2554-2567 (2011).

Shoner, R. G., Ellis, L. F. and Shoner, B. E., The isolation and purification of protein granules from *Escherichia coli* cells overproducing bovine growth hormone. Nature Biotechnology, 3, 151-154 (1985).

Song, L., Flux decline in crossflow microfiltration and ultrafiltration: Mechanisms and modeling of membrane fouling. J. Membrane Sci., 139, 183-200 (1998).

Stamatakis, K. and Tien, C., A simple model of cross-flow filtration based on particle adhesion. AIChE J., 39, 1292-1302 (1993).

Titchener-Hooker, N. J., Gritisis, D., Mannweiler, K., Olbrich, R., Gardiner, S. A. M., Fish, N. M. and Hoare, M., Integrated process design for producing and recovering proteins from inclusion bodies. BioPharm, 4, 34-38 (1991).

Wiesner, M. R., Veerapaneni, S. and Brejchova, D., Improvement in Microfiltration Using Coagulation Pretreatment. Klute, R. and Hahn, H. H., Eds., Proceedings of the Fifth Gothenburg Symposium on Chemical Water and Wastewater Treatment II, Nice, France, Springer, p. 20-40, New York (1992). [*apud* Lim and Bai (2003).]

APPENDIX

In this section, a theoretical derivation of the expression for the age-distribution function given by Eq. (10) is provided. Let S (assumed to be constant) be the fraction of surface elements renewed in a particular age fraction per unit time. In a time interval Δt, one therefore has:

$$S\Delta t = \frac{f(t,t_p)\Delta t - f(t+\Delta t,t_p)\Delta t}{f(t,t_p)\Delta t} = \frac{f(t,t_p) - f(t+\Delta t,t_p)}{f(t,t_p)} \tag{A1}$$

Letting $\Delta t \rightarrow 0$ in the above equation gives:

$$\frac{\partial f}{\partial t} = -Sf \tag{A2}$$

which has to be solved subject to the condition that:

$$\int_o^{tp} f(t,t_p)dt = 1 \tag{A3}$$

From Eqs. (A2) and (A3), it may be shown that:

$$f(t,t_p) = \frac{Se^{-St}}{1-e^{-Stp}} \tag{A4}$$

which is the same as Eq. (10).